

PAPER • OPEN ACCESS

Strain-induced doping and zero line mode at the fold of twisted Bernal-stacked bilayer graphene

To cite this article: Sung Ju Hong *et al* 2021 *2D Mater.* **8** 045009

View the [article online](#) for updates and enhancements.

You may also like

- [Electronic properties of twisted multilayer graphene](#)
V Hung Nguyen, Trinh X Hoang and J-C Charlier
- [Nonlinear anomalous Hall effects probe topological phase-transitions in twisted double bilayer graphene](#)
Atasi Chakraborty, Kamal Das, Subhajit Sinha et al.
- [Interfacial and electrical properties of nanolaminated HfO₂/Al₂O₃ dielectrics on GaN with an AlN interlayer](#)
Hogyoung Kim, Hee Ju Yun, Seok Choi et al.

2D Materials



PAPER

OPEN ACCESS

RECEIVED
12 May 2021

REVISED
6 July 2021

ACCEPTED FOR PUBLICATION
16 July 2021


PUBLISHED
18 August 2021

Original Content from this work may be used under the terms of the [Creative Commons Attribution 4.0 licence](https://creativecommons.org/licenses/by/4.0/).

Any further distribution of this work must maintain attribution to the author(s) and the title of the work, journal citation and DOI.



Strain-induced doping and zero line mode at the fold of twisted Bernal-stacked bilayer graphene

Sung Ju Hong^{1,5,*} , Xiao Xiao¹, Dirk Wulferding^{2,3,4} , Christopher Belke¹, Peter Lemmens² and Rolf J Haug¹ 

¹ Institut für Festkörperphysik, Leibniz Universität Hannover, Hannover 30167, Germany

² Institute for Condensed Matter Physics, TU Braunschweig, Braunschweig 38106, Germany

³ Center for Correlated Electron Systems, Institute for Basic Science (IBS), Seoul 08826, Republic of Korea

⁴ Department of Physics and Astronomy, Seoul National University (SNU), Seoul 08826, Republic of Korea

⁵ Present address: Division of Science Education, Kangwon National University, Chuncheon 24341, Republic of Korea.

* Author to whom any correspondence should be addressed.

E-mail: hong@nano.uni-hannover.de

Keywords: folding, twisted double-bilayer graphene, Bernal stacking, strain-induced doping, zero line mode

Abstract

The folding of Bernal-stacked bilayer graphene leads to electronic devices that can be understood as combinations of a twisted double-bilayer graphene and a fold. In magnetotransport experiments contributions of the two different parts can be identified. For the twisted double-bilayer graphene Landau fan diagrams with satellite fans depending on twist angle are observed. The fold gives rise to a local minimum in conductance which does not shift with applied perpendicular magnetic field. Regardless of twist angle the fold favors electron doping attributed to compressive strain at the kink geometry. The curvature of the folded structure provides for a systematic explanation, which is also in agreement with the observed correlation between twist angle and interlayer distance. Finally, the appearance of the topological zero line mode formed at the fold is discussed.

1. Introduction

The folding of two-dimensional (2D) materials can modify drastically their electronic properties [1–3]. The folded region acts as an interface between the upper and lower layer, so that new topological phenomena appear. Folded graphene can be obtained during mechanical exfoliation [2, 4] as well as by atomic force manipulation [2, 5–8], and self-assembly methods [9–12]. Folded structures consist of two parts: the stacked and the folded region. For monolayer graphene (MLG) the stacked region shows the electronic properties of typical twisted structures [2, 13, 14], whereas for the folded region snake states [15, 16] are expected. Similar to twisted bilayer graphene (tBLG) fabricated by transfer methods [17–23], typical electronic properties such as Fermi velocity renormalization [4, 14], Berry phase transition [4], and superlattice structures [2] were observed in folded MLG layers. Furthermore, an additional peak in the resistance at a certain charge carrier density was attributed to the folded structure [2, 11] due to its independence on applied magnetic field.

Given that folding can provide for a sharp interface overcoming limits of conventional lithography, it can be adopted to realize new topological states. A representative phenomenon is the so-called zero line mode (zLM) in Bernal-stacked BLG where chiral edge states originate from different valleys [24–26]. It has been reported that the zLM can be formed by folding of Bernal-stacked BLG [27, 28]. Therefore, double bilayer graphene (DBLG) formed by folding of Bernal-stacked BLG becomes an important platform to investigate (a) superlattice related phenomena from stacked region and (b) topological phenomena from folded region.

Here, we investigate the magnetotransport properties of folded DBLG. As in tBLG Landau fan diagrams depending on twist angle between the upper and lower BLG are obtained. In addition, a magnetic-field-independent feature as an electrical signature of folding is observed, exhibiting electron doping behavior and topological transport related with zLM. Combining structural and electrical studies, we reveal (a) the origin of the electron doping in terms of lattice deformation, compressive strain, and (b) a structural

correlation between twist angle and interlayer distance, which can provide for an additional base in the emerging research field of twistrionics [29].

2. Experimental section

The folded DBLGs discussed here were obtained during the mechanical exfoliation process. The red-filtered contrast in optical microscopy helps to identify the constituent bilayer graphene. In addition, we used a Raman microscope (LabRam, Horiba) with a laser at an excitation wavelength of 532 nm and ambient conditions to pin down the Bernal stacking. The devices have been encapsulated by hexagonal boron nitride (h-BN from HQ Graphene) [30] and the entire heterostructures are located on SiO₂ (330 nm)/Si substrates. For all heterostructures studied each h-BN layer has been intentionally misaligned to exclude any coupling between the graphene layers and the h-BNs. We have annealed all devices with forming gas (5% H₂ and 95% N₂) at 350 °C and performed atomic force microscopy (AFM) measurement to select bubble-free regions. A SF₆ reactive ion etching process was performed to allow for metal electrodes with atomic edge-contact configuration. By applying a back-gate voltage (V_{bg}) to the backside of the device the charge carrier densities (n) of the graphene heterostructures are modulated. Top-gate (TG) voltages were kept to be ground during all measurements. Electrical experiments have been carried out by low frequency AC or DC methods. All transport measurements have been done in a variable-temperature cryostat equipped with a superconducting magnet.

3. Results and discussion

Figure 1(a) shows schematic images of our folded DBLG. The upper panel shows the folded structure with the constituent Bernal-stacked BLGs twisted by the angle (θ). The folded DBLG consists of two distinct regions (i.e. folded edge and twisted bulk) as shown in the lower panel of figure 1(a). An external magnetic field (B) is applied perpendicular to the planar surface and the electrical current flows along both the stacked and the folded region. The external magnetic field effectively acts as being perpendicular to the stacked region and being parallel to the folded region as shown in the lower panel of figure 1(a). Furthermore, a uniform field applied to the folded layers is equivalent to opposite fields on spatially distinct regions as shown in figure 1(b) giving origin to snake states [15, 16] under applied magnetic fields and zLMs [24–28] under applied electric fields (E). Such a folded region should provide a sharp interface on a scale of few nanometers being much sharper than typical interfaces which can be generated by lithographical methods.

We present here results about two representative devices, one device with a large twist angle (device 1) and one device with a small twist angle (device 2). An AFM image of device 1 is shown in the lower panel of figure 2(a) together with a height profile giving a height of 2.4 nm. A corresponding schematic image is depicted in the upper panel of figure 2(a), where the blue triangular region indicates the folded DBLG. We used the relation $\theta = 2\varphi$ between twist angle (θ) and folding angle (φ) (see the upper panel of figure 2(a)) to estimate the twist angle to $\theta \approx 28^\circ$ [2]. Having folded Bernal-stacked graphene was confirmed by the 2D peak of the Raman spectrum (see inset of figure 2(b)) [31], which is fitted by four Lorentzians (gray curves). The 2D peak stems from double-resonance processes, which can be used as a finger-print for the number of layers and the stacking order [31, 32]. MLG or tBLG with large twist angle exhibits only a single Lorentzian peak, while for Bernal-stacked graphene four Lorentzian peaks are typically seen.

Figure 2(b) also shows the gate-voltage dependent conductance (G) of device 1 at 0 T. A charge neutrality point (CNP) appears as a large dip at $V_{bg} \approx -10$ V (blue square) and an additional small dip is present at $V_{bg} \approx -4$ V (red-dotted arrow). The two conductance minima exhibit different dependencies on magnetic field. The position of the conductance minimum originating from the fold is more or less independent on magnetic field (red-dotted arrows in figure 2(c)), whereas from the CNP a Landau fan originates (blue square). Blue-dashed lines in figure 2(c) correspond to total filling factors $\nu = \pm 4, \pm 8$, where the observed sequences of ν can be understood by the asymmetric doping between upper and lower layers [4, 13, 14, 22, 33–35] due to the application of only back-gate voltages. When two layers are symmetrically doped, the total filling factor ($\nu_{upper} + \nu_{lower}$) is supposed to exhibit 8 (4 + 4), 16 (8 + 8), 24 (12 + 12),... for DBLG. However, the sequence of 4, 8 is expected to originate from (0 + 4), (4 + 4) because the upper layer is relatively less doped due to screening by the lower layer. Satellite dips from superlattice structures are not observed and are also not expected in case of such a large twist angle.

Figure 3(a) shows an AFM image of the second device (device 2) with a height profile giving a height of 2.0 nm for this folded DBLG. A clear bump-like structure as commonly observed in the tBLGs [36] does not appear at the fold of our folded DBLG similar to device 1. Compared to the tBLG, the DBLGs seem to be more consistent with the simple geometry without bumps hinting towards DBLGs being more rigid than MLG. The gate-voltage dependent conductance (G) of device 2 at 0 T is shown in figure 3(b). Local conductance minima which are identified by their magnetic field dependence are seen at $V_{bg} \approx -24$ V (CNP), $V_{bg} \approx -40$ V (folded signature), $V_{bg} \approx 2$ V (first satellite point,

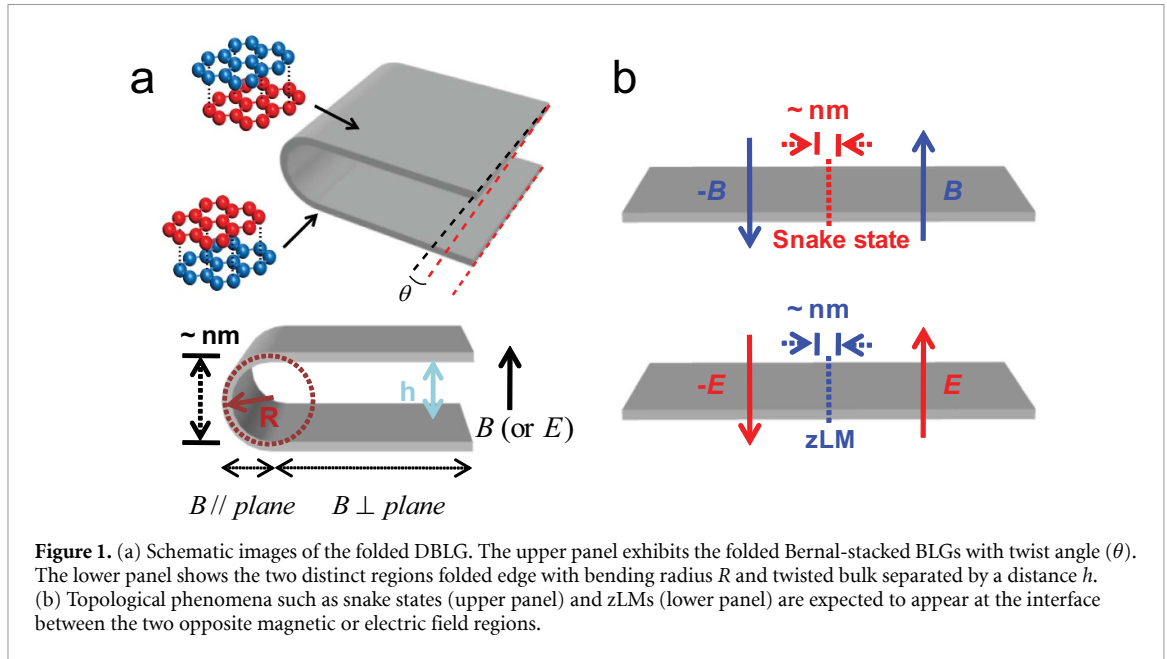


Figure 1. (a) Schematic images of the folded DBLG. The upper panel exhibits the folded Bernal-stacked BLGs with twist angle (θ). The lower panel shows the two distinct regions folded edge with bending radius R and twisted bulk separated by a distance h . (b) Topological phenomena such as snake states (upper panel) and zLMs (lower panel) are expected to appear at the interface between the two opposite magnetic or electric field regions.

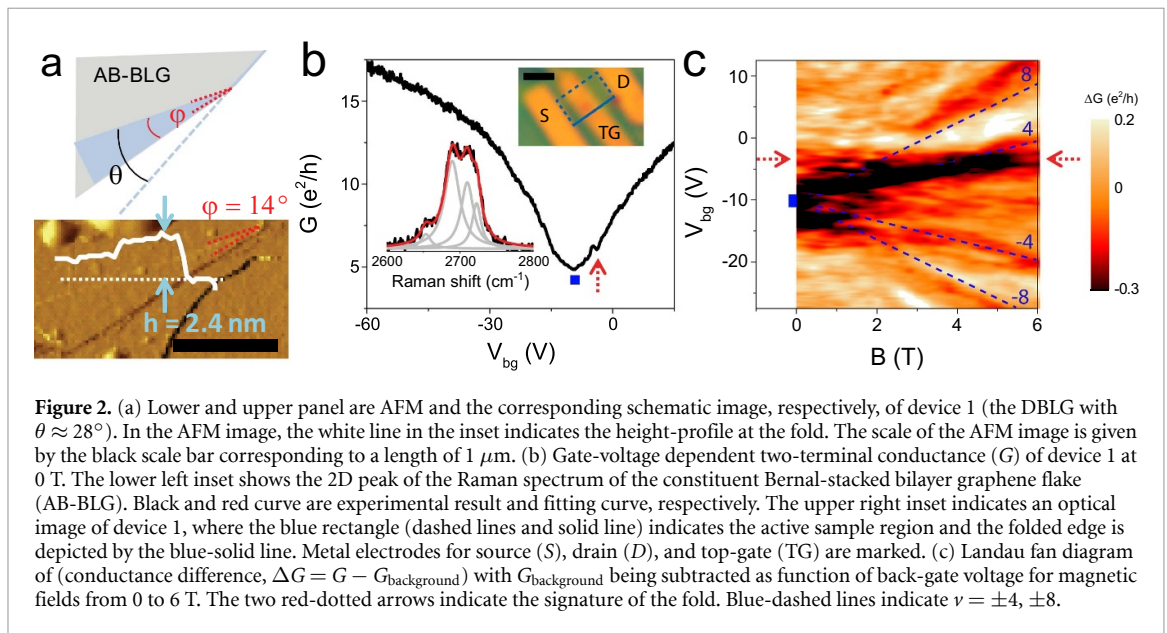
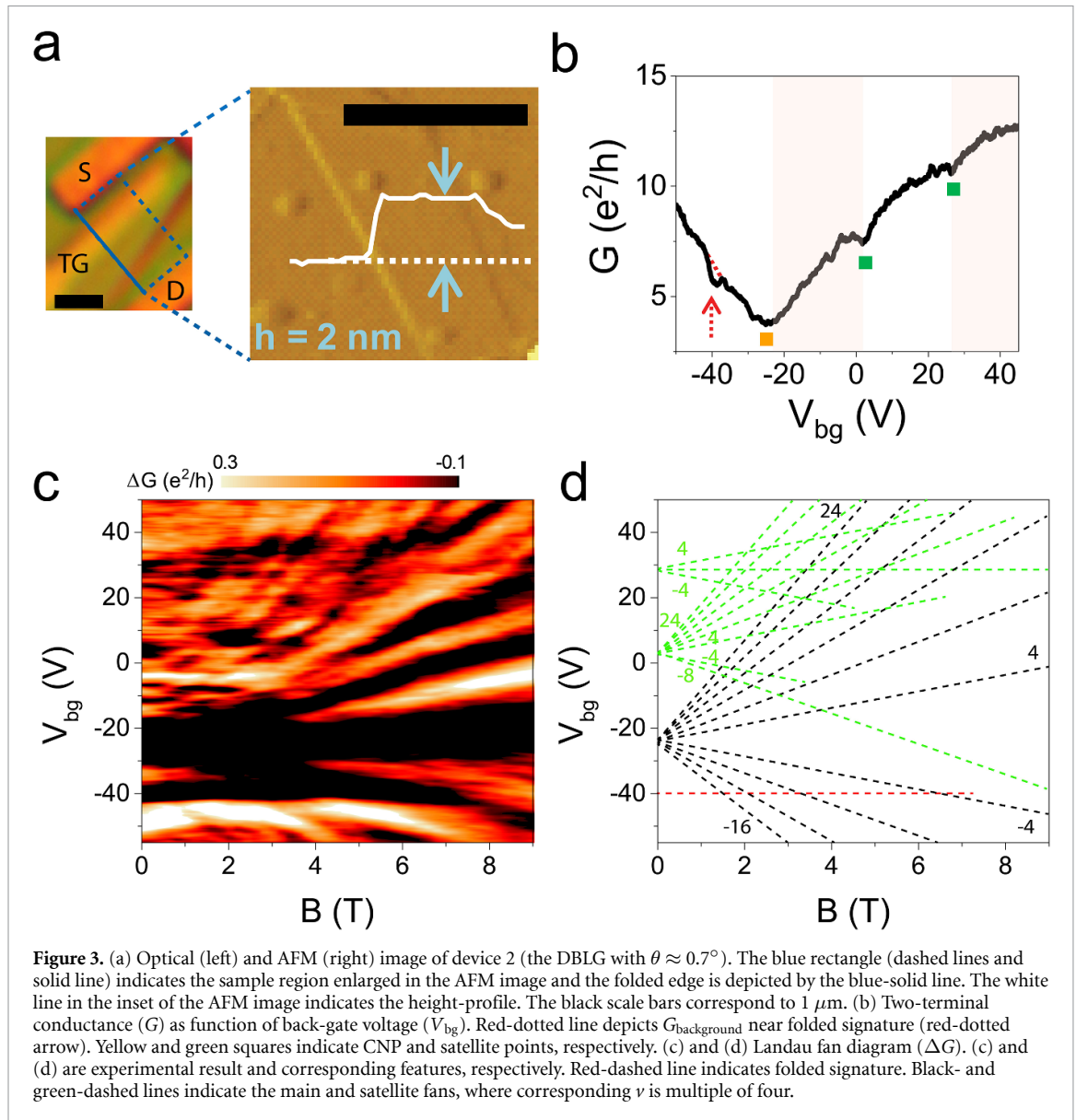


Figure 2. (a) Lower and upper panel are AFM and the corresponding schematic image, respectively, of device 1 (the DBLG with $\theta \approx 28^\circ$). In the AFM image, the white line in the inset indicates the height-profile at the fold. The scale of the AFM image is given by the black scale bar corresponding to a length of $1 \mu\text{m}$. (b) Gate-voltage dependent two-terminal conductance (G) of device 1 at 0 T . The lower left inset shows the 2D peak of the Raman spectrum of the constituent Bernal-stacked bilayer graphene flake (AB-BLG). Black and red curve are experimental result and fitting curve, respectively. The upper right inset indicates an optical image of device 1, where the blue rectangle (dashed lines and solid line) indicates the active sample region and the folded edge is depicted by the blue-solid line. Metal electrodes for source (S), drain (D), and top-gate (TG) are marked. (c) Landau fan diagram of (conductance difference, $\Delta G = G - G_{\text{background}}$) with $G_{\text{background}}$ being subtracted as function of back-gate voltage for magnetic fields from 0 to 6 T . The two red-dotted arrows indicate the signature of the fold. Blue-dashed lines indicate $\nu = \pm 4, \pm 8$.

$n \approx 1.12 \times 10^{12} \text{ cm}^{-2}$), $V_{\text{bg}} \approx 27 \text{ V}$ (second satellite point) depicted by a yellow square, a red-dotted arrow, and two green squares, respectively. Figures 3(c) and (d) show the magnetotransport results (ΔG) and the corresponding features, respectively where the main Landau fan (black-dashed lines), the folded structure (red-dashed line), and the two satellite fans (green-dashed lines) are depicted. Filling factors depicted by black-dashed lines in figure 3(d) are multiples of four, similar to the asymmetric doping between upper and lower layers for device 1. However, the multiples of four in filling factors for device 2 can be attributed to the influence of the Moiré potential; in other words, the folded DBLG with small twist angle can be regarded as a single sys-

tem which possesses a nontrivial Berry curvature of the flat bands [37]. The satellite features occur when the superlattice (Moiré) unit cell is fully occupied. As a result, we extract a twist angle $\theta \approx 0.7^\circ$, from the superlattice density, $n = 4/A_{\text{SL}}$, unit cell area $A_{\text{SL}} = \sqrt{3}/2\lambda_{\text{SL}}^2$, and wavelength $\lambda_{\text{SL}} = a/2\sin(\theta/2)$, where a is the lattice constant of AB-BLG, 0.246 nm . Furthermore, weak features for filling factors (multiples of $\nu = 4$) are observed for the two satellite fans in figures 3(c) and (d). It is noteworthy that correlation phenomena such as superconductivity and Mott insulator are not observed in our folded graphene layers in spite of similar twist angle as recently reported twisted DBLG [38–40]. Even though a lower mobility and therefore stronger disorder are mainly considered



to explain the absence of these correlation phenomena, the influence of the folded structure might be also of importance. A recent study has reported that correlated phenomena are sensitively affected by the interlayer interaction (e.g. interlayer spacing) tuned with external pressure [41]. Indeed, the observation that the interlayer distance is connected to the twist angle in folded graphene [36] may reveal the significant role of folding. Namely, the folded structure can play a role as interlayer coupling parameter, which needs to be further investigated.

In the following we will discuss the electronic properties of the fold in more detail. As in device 1 and 2 where the folds showed up at $V_{\text{bg}} \approx -4$ and -40 V, interestingly in the previous observation of a fold for tBLG also a negative value of $V_{\text{bg}} \approx -25$ V was measured [2]. The fact that the folded signatures are always located at negative values of V_{bg} (being independent of the residual doping of the twisted layers which lead to slight variations in the gate-voltage positions of the

CNPs) hints towards a preferential electron doping of the folded region. Since folding produces structural deformations within the layers, the electronic properties of the fold will differ from the properties of the stacked regions. In view of the fact that compressive strain is present at the folded region [42], the electron doping can be explained with the increase of the Fermi level due to a compressed unit cell [43, 44]. In addition to such compressive strain electron accumulation due to the kink geometry is another factor. From electrostatics it is well known that the electron density in a conductor is higher near a kink geometry [45]. The curvature of the folded structure should be an appropriate parameter to estimate the degree of structural deformation. Using the simple geometry for the folded graphene as shown in the lower panel of figure 1(a), the curvature can be described by $\kappa \equiv 1/R = 2/h$, where R and h are the radius of the folded region and the interlayer distance, respectively. The values for the heights h of the DBLGs

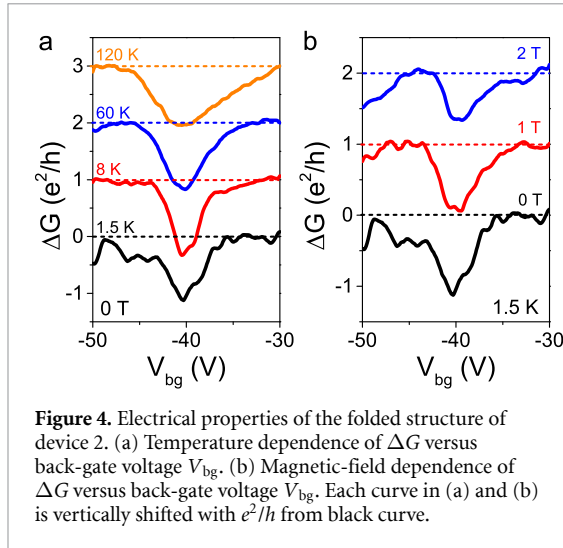


Figure 4. Electrical properties of the folded structure of device 2. (a) Temperature dependence of ΔG versus back-gate voltage V_{bg} . (b) Magnetic-field dependence of ΔG versus back-gate voltage V_{bg} . Each curve in (a) and (b) is vertically shifted with e^2/h from black curve.

are given by the height-profiles as obtained from the AFM measurements.

According to Rode *et al* [36], the twist angle and the interlayer distance of a folded structure are correlated. In our simple model the interlayer distance determines the curvature of the folded structure. Therefore, we compare the amount of electron doping (n_{folded}), interlayer distance (h), curvature (κ), and twist angle (θ). Note that n_{folded} is calculated by a parallel capacitance model using V_{bg} value of the folded signature. The doping concentrations n_{folded} found for device 1 and 2 are $2.5 \times 10^{11} \text{ cm}^{-2}$ and $17 \times 10^{11} \text{ cm}^{-2}$, respectively. Device 1 ($\theta \approx 28^\circ$) and 2 ($\theta \approx 0.7^\circ$) exhibit h of 2.4 and 2.0 nm. Our observation here is in agreement with the correlation between interlayer distance (i.e. curvature of the folded region) and twist angle as found for tBLGs [36]. Even though the interlayer distance is expected to vary non-monotonically as a function of twist angle, two twist angles in this work show consistent results. From the different interlayer distances calculated curvatures κ are given as 0.83 nm^{-1} (device 1) and 1 nm^{-1} (device 2). One sees that the curvature being higher the more electrons are doped in the folded region. In addition, one sees that the smaller twist angle has the higher curvature, which results in a higher doping tendency for smaller twist angles. We note that this trend maintains validity within the tBLG case as previously reported ($n_{\text{folded}} \approx 16 \times 10^{11} \text{ cm}^{-2}$ for $\theta \approx 1.1^\circ$) [2].

Considering the fact that the stacked and folded regions contribute to the entire conductance in parallel in our device, we can extract the electrical properties of the folded structure by subtracting from the two-terminal conductance G the background conductance $G_{\text{background}}$, where $G_{\text{background}}$ might be approximately determined by its bulk part (i.e. the stacked region). Figures 4(a) and (b) show temperature and magnetic-field dependences of the extracted conductance ΔG of the fold of device 2 in such

a way. The depth of the minimum observed in ΔG is around e^2/h inspiring quantized transport via a topological zero-energy mode (or zLM). The minimal conductance seems to be only weakly dependent on temperature, whereas the width of the minimum in ΔG is broadened with increasing temperature hinting towards thermal broadening. While the gate-voltage position of the folded signature is fixed as function of magnetic field, the minimal value of ΔG increases with magnetic field (i.e. decreased depth) as shown in figure 4(b). The suppression of the depth shows that the conductance contributed from the folded region to the total conductance of the device increases. Such an increase in conductance is commonly observed for transitions to chiral edge state transport as it appears for the topological zero-energy mode. Nevertheless, the fact that the electrical signature for the zLM is pinned at certain V_{bg} and has a nearly quantized value indicates the topological robustness of the edge channel emerging in the folded region. Furthermore, quantum interference effects such as weak localization and universal conductance fluctuation might be involved in electrical transport causing. The positive magnetoconductance of the folded region might be influenced by a suppression of weak localization in the regions adjacent to the fold. Even though the direction of the magnetic field is effectively parallel for the kink of the fold, perpendicular components can be locally present. Indeed, a similar positive magnetoconductance was observed in the case of ripples [46] which could represent multiple folds. Also, the weak oscillatory features overlapped on ΔG are suppressed by either elevating temperature (figure 4(a)) or applying magnetic field (figure 4(b)), which may imply the contribution of universal conductance fluctuation.

It is noteworthy that the zLM is expected to be observed regardless of twist angle. Even though we obtained a signature of the fold for device 1 as shown in figure 2(c), a distinction from the Landau fan of the bulk twist system is difficult. Namely, the electrical signatures for the folded region and twisted bulk regions in device 1 are closely located in terms of V_{bg} , preventing further analysis for the zLM of device 1. Because the V_{bg} values are determined by the curvature of the fold and the unintentional doping for folded and twisted bulk regions, respectively, certain conditions for twist angle and unintentional doping could provide for a better observation even in the case of large twist angles.

For tBLGs a clear signature of the fold was achieved within a separate-contact configuration [2], where the electrical current is strongly guided through the folded structure. In the work presented here the stacked and folded regions are connected in parallel, which turns out to be sufficient for detecting transport due to the fold, similar to the recently reported observation of zLM [28]. In order to explore snake states or zLMs in more detail an insulating layer such

as h-BN would help to guide all the current through the fold.

4. Conclusions

In conclusion, we have studied the magnetotransport properties of folded DBLGs with large and small twist angles. In magnetotransport the electronic properties of the stacked and folded regions can be distinguished. The stacked region results in twist-angle dependent Landau fan diagrams. Satellite fans are observed for the small twist angle. This twist-angle dependence hints towards similar new rich physics as already found for tBLGs. The folded region is always electron doped regardless of twist angle. The amount of doping is correlated with the twist angle and the distance between the layers and is attributed to the additional compressive strain due to the folding. In addition, the conductance of the fold which might be related to transport via topological zLMs is studied as function of temperature and magnetic field.

Data availability statement

All data that support the findings of this study are included within the article (and any supplementary files).

Acknowledgments

This work is supported by the Deutsche Forschungsgemeinschaft (DFG, German Research Foundation) under Germany's Excellence Strategy—EXC 2123 Quantum Frontiers—390837967 and within priority program SPP 2244 '2DMP', by the state of Lower Saxony via the School for Contacts in Nanosystems and Fundamentals of Physics and Metrology Initiative. Part of this study has been performed using facilities at the LNQE, Leibniz Universität Hannover, Germany. P L and D W acknowledge support from QUANOMET-NL4 and the Institute for Basic Science (IBS-R009-Y3).

Conflict of interest

The authors declare no competing financial interest.

Author contributions

The experimental concept was conceived by S J H and R J H. S J H, X X, and C B fabricated the devices and performed the transport experiments. D W carried out Raman spectroscopy. S J H and R J H analyzed electrical results. This manuscript was written by S J H, and R J H based on discussions with X X, C B, D W, and P L. All authors have given approval to the final version of the manuscript.

ORCID iDs

Sung Ju Hong  <https://orcid.org/0000-0003-1318-2141>

Dirk Wulferding  <https://orcid.org/0000-0003-4279-2109>

Rolf J Haug  <https://orcid.org/0000-0002-2220-3779>

References

- [1] Kim K, Lee Z, Malone B D, Chan K T, Alemán B, Regan W, Gannett W, Crommie M F, Cohen M L and Zettl A 2011 Multiply folded graphene *Phys. Rev. B* **83** 245433
- [2] Schmidt H, Rode J C, Smirnov D and Haug R J 2014 Superlattice structures in twisted bilayers of folded graphene *Nat. Commun.* **5** 5742
- [3] Qi Z J, Daniels C, Hong S J, Park Y W, Meunier V, Drndić M and Johnson A T C 2015 Electronic transport of recrystallized freestanding graphene nanoribbons *ACS Nano* **9** 3510–20
- [4] Rode J C, Smirnov D, Schmidt H and Haug R J 2016 Berry phase transition in twisted bilayer graphene *2D Mater.* **3** 035005
- [5] Carozo V, Almeida C M, Ferreira E H M, Cançado L G, Achete C A and Jorio A 2011 Raman signature of graphene superlattices *Nano Lett.* **11** 4527–34
- [6] Chen X, Yi C and Ke C 2015 Bending stiffness and interlayer shear modulus of few-layer graphene *Appl. Phys. Lett.* **106** 101907
- [7] Rode J C, Smirnov D, Belke C, Schmidt H and Haug R J 2017 Twisted bilayer graphene: interlayer configuration and magnetotransport signatures *Ann. Phys.* **529** 1700025
- [8] Chang J S, Kim S, Sung H-J, Yeon J, Chang K J, Li X and Kim S 2018 Graphene nanoribbons with atomically sharp edges produced by AFM induced self-folding *Small* **14** 1803386
- [9] Annett J and Cross G L W 2016 Self-assembly of graphene ribbons by spontaneous self-tearing and peeling from a substrate *Nature* **535** 271–5
- [10] Wang B et al 2017 Controlled folding of single crystal graphene *Nano Lett.* **17** 1467–73
- [11] Xu W, Qin Z, Chen C-T, Kwag H R, Ma Q, Sarkar A, Buehler M J and Gracias D H 2017 Ultrathin thermoresponsive self-folding 3D graphene *Sci. Adv.* **3** e1701084
- [12] Bockhorn L, Rode J C, Gnörich L, Zuo P, Brechtken B and Haug R J 2021 Interlayer configurations of self-assembled folded graphene *Appl. Phys. Lett.* **118** 173101
- [13] Schmidt H, Lüdtkke T, Barthold P, McCann E, Fal'ko V I and Haug R J 2008 Tunable graphene system with two decoupled monolayers *Appl. Phys. Lett.* **93** 172108
- [14] Schmidt H, Lüdtkke T, Barthold P and Haug R J 2010 Mobilities and scattering times in decoupled graphene monolayers *Phys. Rev. B* **81** 121403
- [15] Prada E, San-Jose P and Brey L 2010 Zero Landau level in folded graphene nanoribbons *Phys. Rev. Lett.* **105** 106802
- [16] Raimis D, Taddei F, Polini M, León G, Guinea F and Fal'ko V I 2011 Gauge fields and interferometry in folded graphene *Phys. Rev. B* **83** 165403
- [17] Cao Y, Luo J Y, Fatemi V, Fang S, Sanchez-Yamagishi J D, Watanabe K, Taniguchi T, Kaxiras E and Jarillo-Herrero P 2016 Superlattice-induced insulating states and valley-protected orbits in twisted bilayer graphene *Phys. Rev. Lett.* **117** 116804
- [18] Kim Y, Herlinger P, Moon P, Koshino M, Taniguchi T, Watanabe K and Smet J H 2016 Charge inversion and topological phase transition at a twist angle induced

- van hove singularity of bilayer graphene *Nano Lett.* **16** 5053–9
- [19] Kim K, DaSilva A, Huang S, Fallahazad B, Larentis S, Taniguchi T, Watanabe K, LeRoy B J, MacDonald A H and Tutuc E 2017 Tunable moiré bands and strong correlations in small-twist-angle bilayer graphene *Proc. Natl Acad. Sci. USA* **114** 3364–9
- [20] Cao Y, Fatemi V, Fang S, Watanabe K, Taniguchi T, Kaxiras E and Jarillo-Herrero P 2018 Unconventional superconductivity in magic-angle graphene superlattices *Nature* **556** 43–50
- [21] Cao Y *et al* 2018 Correlated insulator behaviour at half-filling in magic-angle graphene superlattices *Nature* **556** 80–4
- [22] Chung T-F, Xu Y and Chen Y P 2018 Transport measurements in twisted bilayer graphene: electron-phonon coupling and Landau level crossing *Phys. Rev. B* **98** 035425
- [23] Hong S J *et al* 2016 Magnetoresistance (MR) of twisted bilayer graphene on electron transparent substrate *Synth. Met.* **216** 65–71
- [24] Martin I, Blanter Y M and Morpurgo A F 2008 Topological confinement in bilayer graphene *Phys. Rev. Lett.* **100** 036804
- [25] Li J, Wang K, McFaul K J, Zern Z, Ren Y, Watanabe K, Taniguchi T, Qiao Z and Zhu J 2016 Gate-controlled topological conducting channels in bilayer graphene *Nat. Nanotechnol.* **11** 1060–5
- [26] Lee J, Watanabe K, Taniguchi T and Lee H-J 2017 Realisation of topological zero-energy mode in bilayer graphene in zero magnetic field *Sci. Rep.* **7** 6466
- [27] Hou T, Cheng G, Tse W-K, Zeng C and Qiao Z 2018 Topological zero-line modes in folded bilayer graphene *Phys. Rev. B* **98** 245417
- [28] Mania E, Cadore A R, Taniguchi T, Watanabe K and Campos L C 2019 Topological valley transport at the curved boundary of a folded bilayer graphene *Commun. Phys.* **2** 6
- [29] Carr S, Massatt D, Fang S, Cazeaux P, Luskin M and Kaxiras E 2017 Twistronics: manipulating the electronic properties of two-dimensional layered structures through their twist angle *Phys. Rev. B* **95** 075420
- [30] Wang L *et al* 2013 One-dimensional electrical contact to a two-dimensional material *Science* **342** 614
- [31] Ferrari A C *et al* 2006 Raman spectrum of graphene and graphene layers *Phys. Rev. Lett.* **97** 187401
- [32] Kim K, Coh S, Tan L Z, Regan W, Yuk J M, Chatterjee E, Crommie M F, Cohen M L, Louie S G and Zettl A 2012 Raman spectroscopy study of rotated double-layer graphene: misorientation-angle dependence of electronic structure *Phys. Rev. Lett.* **108** 246103
- [33] Sanchez-Yamagishi J D, Taychatanapat T, Watanabe K, Taniguchi T, Yacoby A and Jarillo-Herrero P 2012 Quantum Hall effect, screening, and layer-polarized insulating states in twisted bilayer graphene *Phys. Rev. Lett.* **108** 076601
- [34] Fallahazad B, Hao Y, Lee K, Kim S, Ruoff R S and Tutuc E 2012 Quantum Hall effect in Bernal stacked and twisted bilayer graphene grown on Cu by chemical vapor deposition *Phys. Rev. B* **85** 201408
- [35] Kim Y *et al* 2016 Broken-symmetry quantum Hall states in twisted bilayer graphene *Sci. Rep.* **6** 38068
- [36] Rode J C, Zhai D, Belke C, Hong S J, Schmidt H, Sandler N and Haug R J 2018 Linking interlayer twist angle to geometrical parameters of self-assembled folded graphene structures *2D Mater.* **6** 015021
- [37] Wu Q, Liu J, Guan Y and Yazev O V 2021 Landau levels as a probe for band topology in graphene moiré superlattices *Phys. Rev. Lett.* **126** 056401
- [38] Cao Y, Rodan-Legrain D, Rubies-Bigorda O, Park J M, Watanabe K, Taniguchi T and Jarillo-Herrero P 2020 Tunable correlated states and spin-polarized phases in twisted bilayer–bilayer graphene *Nature* **583** 215–20
- [39] Liu X *et al* 2020 Tunable spin-polarized correlated states in twisted double bilayer graphene *Nature* **583** 221–5
- [40] Burg G W, Zhu J, Taniguchi T, Watanabe K, MacDonald A H and Tutuc E 2019 Correlated insulating states in twisted double bilayer graphene *Phys. Rev. Lett.* **123** 197702
- [41] Yankowitz M, Chen S, Polshyn H, Zhang Y, Watanabe K, Taniguchi T, Graf D, Young A F and Dean C R 2019 Tuning superconductivity in twisted bilayer graphene *Science* **363** 1059
- [42] Ortolani L, Cadelano E, Veronese G P, Degli Esposti Boschi C, Snoeck E, Colombo L and Morandi V 2012 Folded graphene membranes: mapping curvature at the nanoscale *Nano Lett.* **12** 5207–12
- [43] Choi S-M, Jhi S-H and Son Y-W 2010 Effects of strain on electronic properties of graphene *Phys. Rev. B* **81** 081407
- [44] He X *et al* 2015 Tuning the graphene work function by uniaxial strain *Appl. Phys. Lett.* **106** 043106
- [45] Cao G, Liu W, Cao M, Li X, Zhang A, Wang X and Chen B 2016 Improve the transconductance of a graphene field-effect transistor by folding graphene into a wedge *J. Phys. D: Appl. Phys.* **49** 275108
- [46] Wakabayashi J and Sano K 2011 Magnetoresistance of bilayer graphene in parallel magnetic fields *J. Phys. Soc. Jpn.* **81** 013702